RSC Advances

PAPER

View Article Online
View Journal | View Issue

Cite this: *RSC Adv.*, 2017, **7**, 2258

Guest dependent structure and acetone sensing properties of a 2D Eu^{3+} coordination polymer†

Meng Zhao,[ac] Zhao-Quan Yao,[ac] Yue-Ling Xu,[ac] Ze Chang*[ac] and Xian-He Bu[abc]

Received 23rd October 2016
Accepted 1st December 2016

DOI: 10.1039/c6ra25681c

www.rsc.org/advances

A new two dimensional (2D) Eu^{3+} coordination polymer, named $[Eu(BTB)(H_2O)_2 \cdot solvent]_n$ (**1**) (H_3BTB = 4,4′,4″-benzene-1,3,5-triyl-tribenzoic acid) has been constructed and investigated for sensing properties. Complex **1** shows structural flexibility originating from the 2D layer architecture, which could be triggered by the removal/restore of coordinated and guest solvent molecules. Benefiting from the high stability and intensive Eu^{3+} based emission of **1**, it could be used as an effective fluorescence sensor for acetone with remarkable anti-interference and recyclability. In addition, the impact of structural features on the sensing performance of the complex was investigated, and enhanced sensing sensitivity was achieved with the desolvated complex.

Introduction

Lanthanide-based coordination polymers (Ln-CPs), as a new type of organic–inorganic hybrid porous material, have been widely studied owing to their diverse structures and versatile applications in different fields such as gas adsorption and separation,[1] magnetic materials,[2] molecular recognition and detection,[3] dye enrichment and separation[4] and so on. Compared with the CPs constructed with transition metal ions, the relatively high coordination affinity of lanthanide ions to oxygen atoms increases the bond energy of Ln–O, which makes the Ln-CPs possess high thermal and chemical stability. Also, the high coordination number of lanthanide ions could benefit the formation of nodes with multiple connections and solvent occupied potential open metal sites, which could result in high dimensional framework structure with unique topology and remarkable gas sorption or sensing properties. In addition, the characteristic fluorescence emissions of lanthanide ions, which are readily detectable and distinguishable for their high intensity and specific emission wavelength, are ideal signals for sensing applications.[5] Based on these advantages mentioned above, Ln-CPs becomes very splendid candidates as fluorescence sensors.

On the other hand, acetone as one kind of common solvent plays a vital role in the production of chemical industry. Besides, it can be used as raw material to produce many chemicals. However, acetone is volatile and too much acetone intake will stimulate the eyes, skin and respiratory tract,[6] and the water solubility of it is excellent, which impose great threat to water areas and aquatic organism, then the hazard could be passed on through water cycle or food chain. Therefore, the effective sensing of acetone is quite necessary for personal and environmental protection purpose.

To date, many Ln-CPs have shown remarkable fluorescent sensing performances toward acetone, and the sensing mechanism has also been well investigated. However, the influence of the structure of the Ln-CPs on their sensing performances has been less investigated. Moreover, most of the reported Ln-CPs sensors possess three dimensional (3D) framework structures (also known as metal–organic frameworks, MOFs) with rigid architecture, while the sensing properties of Ln-CPs with two dimensional (2D) structures has not been explored systematically. Since the coordination polymers with 2D structures could be flexible under certain conditions to present unique guest responsive dynamic behaviors and properties that could improve their recognizing and sensing performances, Ln-CPs with 2D structures can be a candidate sensing platform with great potential.

With our continuous efforts toward the construction of coordination polymers based fluorescent sensors toward acetone,[6b,7] much attention has been paid on the fabrication of Ln-CPs with 2D structures based on the considerations mentioned above, and the relationship between the structure of the 2D Ln-CPs and their sensing performances has been investigated. Herein, the construction and acetone sensing properties of a 2D Ln-CP are reported. By utilizing Eu^{3+} as metal center and 4,4′,4″-benzene-1,3,5-triyl-tribenzoic acid (H_3BTB) (Scheme

[a]*School of Materials Science and Engineering, National Institute for Advanced Materials, TKL of Metal- and Molecule-Based Material Chemistry, Nankai University, Tianjin 300350, China. E-mail: changze@nankai.edu.cn*

[b]*State Key Laboratory of Elemento-Organic Chemistry, College of Chemistry, Nankai University, Tianjin 300071, China*

[c]*Collaborative Innovation Center of Chemical Science and Engineering (Tianjin), Tianjin 300071, China*

† Electronic supplementary information (ESI) available. CCDC 1478661 & crystallographic data in CIF format, crystallographic refinement data, additional structure figures, PXRD, TGA, UV-visible absorption spectrums and adsorption enthalpy data. For ESI and crystallographic data in CIF or other electronic format see DOI: 10.1039/c6ra25681c

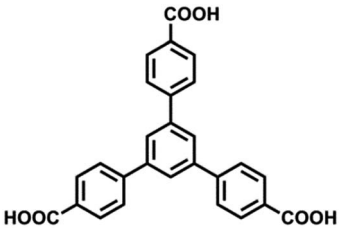

Scheme 1 The H_3BTB ligand used for the construction of **1**.

1) as ligand, a Ln-CP with 2D structure, namely $[Eu(BTB)(H_2O)_2 \cdot solvent]_n$ (**1**), was constructed under solvothermal condition. Complex **1** shows intense Eu^{3+} characteristic fluorescent emission based on the sensitization of BTB^{3-} as "antenna", and the emission could be selectively and effectively quenched by acetone, which makes it a good candidate for acetone detection application. In addition, the structure flexibility of complex **1**, originated from its 2D layer structure and triggered by the loss of guest and coordinated solvent molecules, was also investigated. The desolvated complex **1a** reveals moderate gas storage capacity and enhanced sensitivity toward acetone due to the transformed structure. To the best of our knowledge, this is the first report of the impact of structure features on the sensing performance of 2D Ln-CPs.

Experimental

Materials and methods

All of the materials and reactants are purchase from commercial suppliers without further purification. TENSOR 27 (Bruker) FT-IR spectrometer was used to determine the Infrared spectra by pellet method. The room temperature powder X-ray diffraction (PXRD) spectra were recorded on a Rigaku D/Max-2500 diffractometer at 40 kV, 100 mA with a Cu-target tube and a graphite monochromator and a Rigaku MiniFlex600 diffractometer at 40 kV, 50 mA with a Cu-target tube and a graphite monochromator. Thermogravimetric analyses (TGA) were carried out on a Rigaku standard TG-DTA analyzer with a heating rate of 10 °C min^{-1} from ambient temperature to 700 °C, where an empty Al_2O_3 crucible was used for reference. Gas adsorption measurements were carried out on a ASAP 2020 M surface area and porous analyzer. Fluorescence measurements were performed on a Hitachi F-4500 fluorescence spectrophotometer equipped with a plotter unit. The solid ultraviolet visible absorption spectrums were carried out on a UV-3600 spectrophotometer using $BaSO_4$ as reference substance. UV-Visible absorption spectral measurements were performed on a U-3010 spectrophotometer. Simulation of the PXRD pattern was carried out by the single-crystal data and diffraction-crystal module of the mercury (Hg) program.

Synthesis of $[Eu(BTB)(H_2O)_2 \cdot solvent]_n$ (1) and $[Eu(BTB)]_n$ (1a)

Complex **1** was synthesized through the solvothermal reaction of $Eu(NO_3)_3 \cdot 9H_2O$ (30 mg), H_3BTB (27 mg), and LiCl (20 mg) solved in a mixture of CH_3CN (2 ml), DMF (1 ml) and H_2O (0.3 ml) at 100 °C. Colorless hemiprism crystals were obtained in one day with a yield of 45% based on Eu. FT-IR (KBr pellets, cm^{-1}): 3394.39 m, 2924.95 m, 1660.05 s, 1607.39 s, 1582.91 s, 1533.89 s, 1410.60 s, 1253.32 m, 1186.40 m, 1098.04 m, 1013.66 m, 899.10 w, 960.99 m, 784.96 m, 671.37 m, 478.56 m, 401.13 m.

The sample of **1** was solvent exchanged in CH_3CN for three days and then degassed under high vacuum (less than 10^{-5} Torr) at 220 °C overnight to remove all residue guest in the channels and coordinated water molecules from the framework to give the sample of **1a**. Anal. calcd for $C_{27}H_{15}EuO_6$: C 55.19%, H 2.56%. Found: C 55.05%, H 2.47%, N 0.77%.

Crystallography

The crystal structure of compound **1** was determined by Rigaku 007 Saturn 70 equipped with molybdenum target at 113 K. The program SAINT[8] was used for the integration of diffraction profiles. The program CrystalClear was used for the integration of the diffraction profiles. Program SHELXTL[9] was used to solve structure directly. The hydrogen atoms were added theoretically, riding on the concerned atoms. It should be noted that the highly disordered guest molecules in the compounds cannot be modeled properly, and therefore the corresponding diffused electron densities were removed by the SQUEEZE routine in PLATON[10] (the results were appended in the CIF files†). Crystal data and structure refinement parameters of **1** were listed in Table S1,† with some selected bond lengths and angles collected in Table S2.†

Determination of sensing properties

The emission quenching behaviors of complex **1** toward different solvents were applied to evaluate its selectivity to acetone. In a typical experimental, 3 mg of **1** was dispersed in 3 ml solvent by ultrasound, forming a suspension and then aged for 3 hours. The turbid liquid was then transfer into quartz colorimetric utensil and recorded the emission spectrum between 450 to 750 nm under excitation light source with a wavelength at 310 nm.

The sensing recyclability of the complex was evaluated with the following procedure: for one cycle, 3 mg of **1** was dispersed in 3 ml ethanol and recorded for its emission intensity, and then 0.5 ml acetone was added to quench the emission. After that, the supernatant liquid was removed by centrifuge and the solid was washed thoroughly with ethanol and dispersed in 3 ml fresh ethanol for emission intensity record again.

Results and discussion

Structure description of complex 1

Single crystal X-ray diffraction analysis shows that complex **1** crystallizes in $P\bar{1}$ space group. As shown in Fig. 1a, the asymmetric unit of **1** is composed of one Eu^{3+}, one BTB^{3-} and two water molecules. Thus, the framework is uncharged by analyzing of molecular formula. There is only one type of Eu^{3+} ion in **1** with nine coordinated sites occupied by oxygen atoms. For all the coordinating oxygen atoms, seven of them belong to four carboxylate groups from different BTB^{3-} ligands, showing

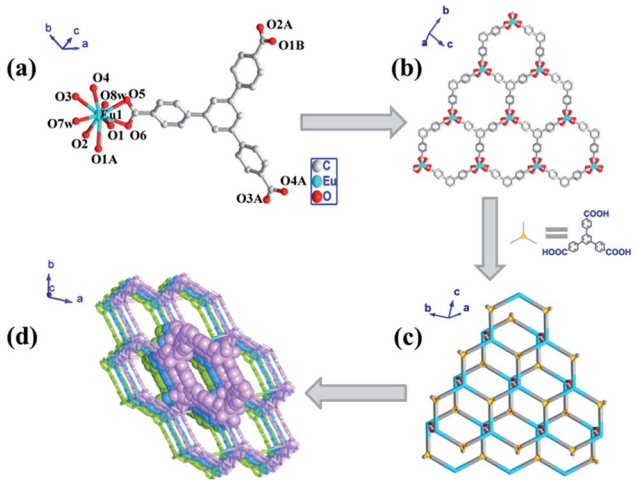

Fig. 1 The crystal structure of **1**. (a) The coordination environment of Eu1 and BTB^{3-} (b) the 2D layer structure (c) the illustration of the bilayer structure. (d) The 1D hexagonal channel viewing from *c* direction forming from stacking of 2D bilayer along *c* direction.

chelating-bridge mode (O1 and O2, O1A) and chelating mode (O3 and O4, O5 and O6). The rest two sites are occupied by O atoms from terminal water molecules (O7W and O8W). The bond length of Eu–O falls in 2.40–2.70 Å. Through the bridging of BTB^{3-} ligands, the Eu^{3+} ions are connected to result in 2D networks (Fig. 1b). Each 2D network is further connected to a neighboring one through the bridging of O1, and stable laminate bilayers were formed (Fig. 1c). One dimensional (1D) channels (~11.4 × 9.6 $Å^2$, regardless of the van der Waals radius) were formed from the stacking of bilayers along *c* direction, which is filled with guest solvent molecules (Fig. 1d). The accessible volume of complex **1** was calculated to be 43.8% in respect to the cell volume after the removal of guest solvent and 50.9% after the removal of coordinated water molecules, which indicates its potential in the accommodation of guest molecules. It is worth noticing that all the previously reported Ln-CPs based on BTB^{3-} ligand show 3D frameworks. Then complex **1** presents the first example of BTB^{3-} based Ln-CPs with 2D structure.

Stability and porosity

Powder X-ray diffractions were performed to identify the phase purity of complex **1** (Fig. S1†). The pattern of the as-synthesized sample matches that of the simulated one calculated from the crystal structure, which indicates the sample possesses high phase purity and provides convenient for further study of its properties.

The stability of complex **1** was characterized to evaluate it potential of properties investigations and applications. The thermostability of complex **1** was characterized by TGA (Fig. S2†). The thermogravimetric profile of complex **1** reveals continuous loss of weight (36.4%) before the reach of relatively stable state at about 260 °C, which should be attributed to the removal of guest solvents and coordinated water molecules from the network of **1**. Then the profile shows a platform between 260–450 °C before the decomposition of the framework, which indicates that the framework can keep stable under high temperature. The remarkable stability of complex **1** should be attributed to the relatively robust nature of Eu–O bonds. On the other hand, the stability of complex **1** toward solvents were verified by examining the PXRD patterns of the samples soaked in different solvents for 2 days (Fig. S4†). These patterns match that of the as prepared sample of complex **1** well, suggesting the good stability of the complex.

Furthermore, the porosity and gas sorption performances of complex **1** were also investigated considering its porous structure, and the entirely desolvated sample **1a** was used for gas sorption experiments. It should be noted that though some peaks were missed in the PXRD pattern of **1a** compared with that of the as synthesized **1**, re-soaking the desolvated sample into mother liquid could make it restore (Fig. S5†). This should be attributed to the flexibility of the structure response to the removal and restore of guest solvents.

For pore structure characterization of **1a**, N_2 absorption isotherms were collected at 77 K in liquid nitrogen bath. The N_2 isotherms show typical type I behavior, indicating the microporous structure of **1a** (Fig. 2a). From the N_2 adsorption isotherm, the Brunauer–Emmett–Teller (BET) and Langmuir surface area are calculated to be 338 $m^2\ g^{-1}$ and 447 $m^2\ g^{-1}$, respectively. The pore width mainly distribute within the range 5–8 Å calculated by Horvath–Kawazoe method (Fig. S6†), relatively smaller than that determined from the crystal structure. The differences between the theoretical and experimental pore dimensions should also be attributed to the changed structure of **1a** compared with that of **1**. Furthermore, the capacity of **1a** toward CO_2 and CH_4 were investigated since porous CPs could be effective platform for CO_2 capture and CH_4 storage. As shown in Fig. 2b, the uptake of CO_2 reaches 40.1 $cm^3\ g^{-1}$ at 273 K under 1 atm and 25.9 $cm^3\ g^{-1}$ at 298 K under 1 atm, while the CH_4 uptakes are 17.1 $cm^3\ g^{-1}$ and 9.8 $cm^3\ g^{-1}$ under the corresponding conditions, respectively. Based on the isotherms, the initial isosteric heat of sorption (Q_{st}) estimated using the virial method is about 27.5 kJ mol^{-1} for CO_2 and 21.5 kJ mol^{-1} for CH_4 (Fig. S7†). The relatively high Q_{st} observed indicates a stronger interaction between the framework and the adsorbed

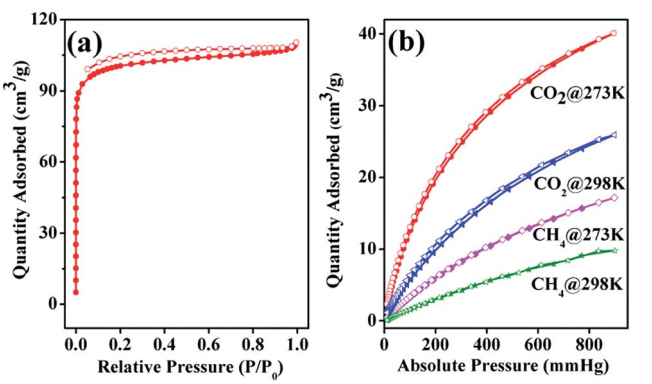

Fig. 2 (a) The N_2 isotherms of **1a** at 77 K. (b) The CO_2 and CH_4 isotherms of **1a** at different temperatures. The filled and open symbols present for adsorption and desorption data, respectively.

gas molecules, which might be attributed to the presence of unsaturated metal sites in the framework after the removal of coordinated water molecules and the confined pore dimension.

Fluorescent sensing property

As mentioned in the introduction, Ln-CPs could be ideal candidate for the sensing of acetone. Therefore, the sensing performance of **1** and **1a** toward acetone were investigated.

Firstly, the emission properties of **1** and **1a** were characterized. As shown in Fig. 3 and S3,† the solid fluorescence spectra of both **1** and **1a** shown characteristic emission peaks of Eu^{3+} under excitation at 310 nm. The peaks at 538 nm, 554 nm, 592 nm, 621 nm, 651 nm, and 698 nm could be assigned to $^5D_1 \rightarrow {}^7F_1$, $^5D_1 \rightarrow {}^7F_2$, $^5D_0 \rightarrow {}^7F_1$, $^5D_0 \rightarrow {}^7F_2$, $^5D_0 \rightarrow {}^7F_3$, and $^5D_0 \rightarrow {}^7F_4$ transitions,[5j] respectively. In contrast, no emission of BTB^{3-} ligand was observed. These results indicate that the BTB^{3-} ligand mainly acts as "antenna" for the sensitizing of Eu^{3+} ions, which agree well with the UV-Visible spectra of **1** (Fig. S8†). On the other hand, the emission intensity of **1a** is higher compared with that of **1**. Considering about their differences in component and structure, the enhanced emission intensity of **1a** should be attributed to the elimination of coordinated water from Eu^{3+} centers, of which the vibration of O–H could quench the fluorescence emission of Ln ions.[11] These results suggested that the emissions of these complexes are highly structure and component dependent, which motivated us for the further investigation of their sensing performances.

Furthermore, the acetone sensing performances of **1** was investigated. As expected, the emission of **1** at 621 nm could be quenched effectively by acetone compared with other solvents (Fig. 4a), which indicated that **1** shows high sensing selectivity toward acetone. And a good anti-interference capability of **1** has been shown in Fig. 4b. In order to explore the relationship between the fluorescence change and the content of acetone, titration experiments were performed with ethanol as solvent. As shown in Fig. 5, with the raise of the content of acetone in the ethanol solvent, the intensity of the emission of **1** at 621 nm drops gradually, and the quenching efficiency reaches 80% at 6% (vol%). These results are comparable with that of some reported complexes used for acetone sensing application.[12] In addition, the recyclability of **1** for sensing was evaluated since

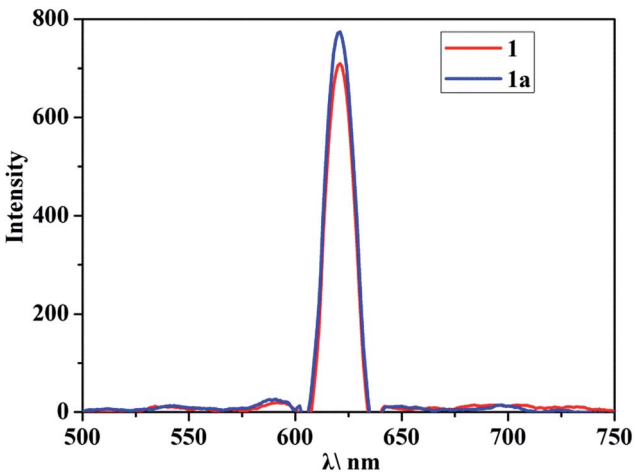

Fig. 3 Solid state fluorescent spectra of **1** and **1a** under excitation at 310 nm.

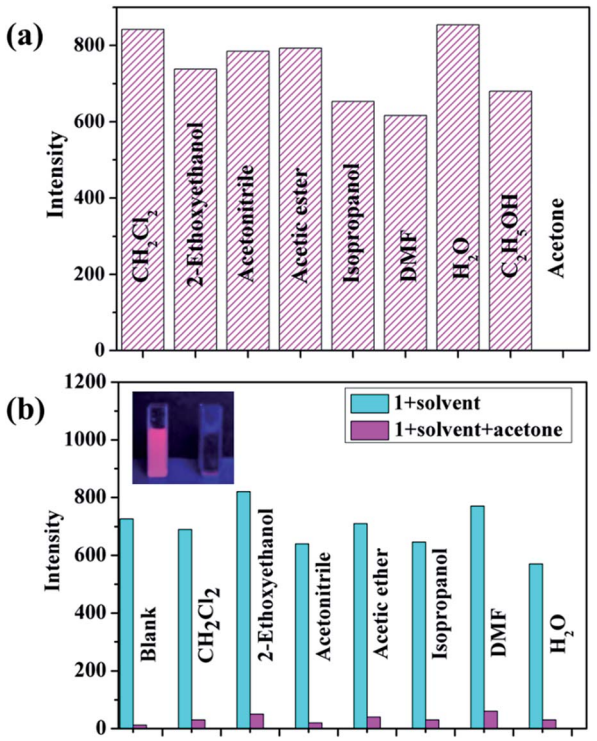

Fig. 4 (a) The fluorescent response of **1** toward different solvents. (b) The fluorescent intensities of **1** in ethanol with the addition of 500 μl different organic solvents (cyan) and the intensities after addition of 500 μl acetone (magenta), (inset: the photo of blank before (left) or after (right) the addition of acetone).

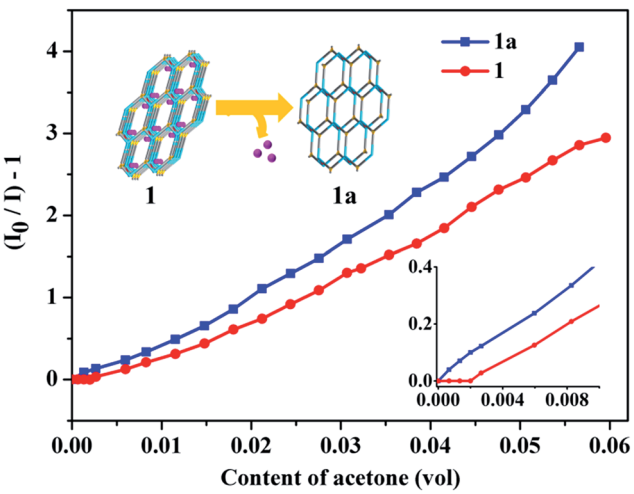

Fig. 5 The structure dependent sensing performances of **1** and **1a** presented by the relationship between quenching efficiency and acetone content in ethanol calculated from emission at 621 nm. The I_0 and I present for the initial and quenched intensity of emission, respectively. The inset represents the quenching performances of **1** and **1a** at low concentration.

this could be a critical factor for potential application. There was no obvious decrease of the emission intensity of **1** even after 10 cycles of sensing (Fig. S9†). The PXRD pattern of the recycled sample matched that of the simulated results well (Fig. S10†), indicating the preservation of high crystallinity after recycles. The remarkable sensing performances and stability of **1** makes it a good candidate for acetone sensing.

The quenching mechanism was further studied. From the UV-Visible spectra of different solvents (Fig. S8†), it was found that only the absorption of acetone overlap with that of complex **1** well, which could result in a competition in the absorption of excitation energy between the acetone and **1**, that is, acetone may absorption the energy that should be used to excited complex **1** for emission. Therefore, the highly selective fluorescence quenching of **1** under acetone conditions might be attributed to competitive absorption mechanism.

Impact of structure features on sensing performance

Based on the determination of the acetone sensing performances of **1**, the sensing property of **1a** was also studied to illustrate the impact of structure features on the sensing performances. In contrast to the enhanced emission intensity of **1a** compared to **1** in solid state, the emission intensity of **1a** in ethanol is weaker than that of **1**. However, when comparing the acetone quenching efficiency of **1** and **1a** at high concentration based on Stern–Volmer (SV) equation[13] (Fig. S11†), the relatively larger K_{sv} of **1a** (47.6) compared to that of **1** (42.6) indicates the enhanced sensitivity of **1a** toward acetone (Fig. 5). More importantly, the detection limit is determined to be 0.3% for **1**, while that for **1a** is as low as 0.01% under the same condition (Fig. 5 inset). These results indicate that **1a** exhibit remarkably enhanced acetone sensing performances to that of **1**.

In order to explain the results, the PXRD patterns of **1a** and the sample after soaked in ethanol were measured and studied (Fig. S12†). Compared to the as synthesized PXRD pattern of **1**, the peak corresponding to (1, 0, 1), (0, 1, −2), (1, 1, 0) lattice planes show some shift to high angle direction in that of **1a**, indicating the occurrence of lattice planes slide in response to the removing of coordinated water molecules and guest solvent molecules. Furthermore, when **1a** was soaked in ethanol, the corresponding peaks disappeared, indicating the loss of long range order. According to these results we speculated that the desolvation process triggers the slide of layers structure. Then, when the desolvated **1a** was soaked in ethanol, solvent molecules interact with the layers and the interaction between layers was broken completely. In this case, the decreased emission intensity of **1a** in ethanol should be attributed to the decreased rigidity of the layer structure without the inter-layer interactions, which will benefit the non-radiation relaxation process to quench the emission. On the other hand, the reduced interlayer interaction in **1a** would make it disperse in ethanol and interacted with guest more effectively than **1**, which will result in the enhanced sensing sensitivity even at low concentration. These results show that the structure flexibility of 2D Ln-CPs may have intense impact on their sensing performances, which might be utilized for the modulation of the properties.

Conclusions

In summary, a new 2D porous Eu^{3+} CP has been constructed based on BTB^{3-} ligand, which reveals remarkable fluorescent sensing properties toward acetone with considerable selectivity and recyclability originated from its unique emission properties and structure stability. Moreover, structure flexibility induced by the removal/restore of coordinated and guest solvent molecules in the porous framework based on 2D layers shows strong impact on the sensing sensitivity of the complex. These results could be instructive for the performances targeted construction of CPs based sensing materials.

Acknowledgements

This work was supported by 973 Program of China (2014CB845601), the National Science Foundation of China (21290171, 21421001, and 21671112), MOE Innovation Team of China (IRT13022), and Natural Science Fund of Tianjin, China (16JCQNJC02400).

References

1 (*a*) X. Peng and D.-P. Cao, *AIChE J.*, 2013, **59**, 2928; (*b*) Q. Liu, J.-M. Yang, F. Guo, L. N. Jin and W.-Y. Sun, *Dalton Trans.*, 2016, **45**, 5841; (*c*) J.-H. Luo, H.-W. Xu, Y. Liu, Y.-S. Zhao, L. L. Daemen, C. Brown, T. V. Timofeeva, S.-Q. Ma and H.-C. Zhou, *J. Am. Chem. Soc.*, 2008, **130**, 9626; (*d*) L. Pan, K. M. Adams, H. E. Hernandez, X.-T. Wang, C. Zheng, Y. Hattori and K. Kaneko, *J. Am. Chem. Soc.*, 2003, **125**, 3062; (*e*) P.-P. Cui, X.-D. Zhang, Y. Zhao, A.-Y. Fu and W.-Y. Sun, *Dalton Trans.*, 2016, **45**, 2591.

2 (*a*) X.-J. Zhang, V. Vieru, X.-W. Feng, J. L. Liu, Z.-J. Zhang, B. Na, W. Shi, B.-W. Wang, A. K. Powell, L. F. Chibotaru, S. Gao, P. Cheng and J.-R. Long, *Angew. Chem., Int. Ed.*, 2015, **54**, 9861; (*b*) J.-W. Zhang, X.-M. Kan, B.-Q. Liu, G.-C. Liu, A.-X. Tian and X.-L. Wang, *Chem.–Eur. J.*, 2015, **21**, 16219; (*c*) J. C. G. Bunzli, *J. Coord. Chem.*, 2014, **67**, 3706.

3 (*a*) Z.-H. Xiang, C.-Q. Fang, S.-H. Leng and D.-P. Cao, *J. Mater. Chem. A*, 2014, **2**, 7662; (*b*) J. Sahoo, R. Arunachalam, P. S. Subramanian, E. Suresh, A. Valkonen, K. Rissanen and M. Albrecht, *Angew. Chem., Int. Ed.*, 2016, **55**, 9625; (*c*) Z.-Q. Li, P. Li, Q.-Q. Xu and H.-R. Li, *Chem. Commun.*, 2015, **51**, 10644; (*d*) D. Liu, J.-P. Lang and B.-F. Abrahams, *J. Am. Chem. Soc.*, 2011, **133**, 11042; (*e*) X.-Q. Wang, L.-L. Zhang, J. Yang, F.-L. Liu, F. Dai, R.-M. Wang and D.-F. Sun, *J. Mater. Chem. A*, 2015, **3**, 12777; (*f*) M. Schaferling, T. Aaritalo and T. Soukka, *Chem.–Eur. J.*, 2014, **20**, 5298.

4 (*a*) S. Seth, G. Savitha and J. N. Moorthy, *J. Mater. Chem. A*, 2015, **3**, 22915; (*b*) J.-S. Qin, S.-R. Zhang, D.-Y. Du, P. Shen, S.-J. Bao, Y.-Q. Lan and Z.-M. Su, *Chem.–Eur. J.*, 2014, **20**, 5625.

5 (*a*) L.-Z. Yang, J. Wang, A. M. Kirillov, W. Dou, C. Xu, R. Fang, C.-L. Xu and W.-S. Liu, *CrystEngComm*, 2016, **18**, 6425; (*b*) W. P. Lustig, F. M. Wang, S. J. Teat, Z. C. Hu, Q. H. Gong and J. Li, *Inorg. Chem.*, 2016, **55**, 7250; (*c*) W.-S. Liu, T.-Q. Jiao, Y.-Z. Li, Q.-Z. Liu, M.-Y. Tan, H. Wang and

L.-F. Wang, *J. Am. Chem. Soc.*, 2004, **126**, 2280; (*d*) M. D. Allendorf, C. A. Bauer, R. K. Bhakta and R. J. T. Houk, *Chem. Soc. Rev.*, 2009, **38**, 1330; (*e*) Z.-C. Hu, B. J. Deibert and J. Li, *Chem. Soc. Rev.*, 2014, **43**, 5815; (*f*) Y.-J. Cui, H. Xu, Y.-F. Yue, Z.-Y. Guo, J.-C. Yu, Z.-X. Chen, J.-K. Gao, Y. Yang, G.-D. Qian and B.-L. Chen, *J. Am. Chem. Soc.*, 2012, **134**, 3979; (*g*) S.-Y. Zhang, W. Shi, P. Cheng and M. J. Zaworotko, *J. Am. Chem. Soc.*, 2015, **137**, 12203; (*h*) J.-N. Hao and B. Yan, *Chem. Commun.*, 2015, **51**, 14509; (*i*) J.-C. Yu, Y.-J. Cui, C.-D. Wu, Y. Yang, B.-L. Chen and G.-D. Qian, *J. Am. Chem. Soc.*, 2015, **137**, 4026; (*j*) H. Xu, C.-S. Cao and B. Zhao, *Chem. Commun.*, 2015, **51**, 10280; (*k*) Y. Wang, F. Zhang, Z.-S. Fang, M.-H. Yu, Y.-Y. Yang and K. L. Wong, *J. Mater. Chem. C*, 2016, **4**, 8466; (*l*) F. Zhang, Y. Wang, T.-S. Chu, Z.-H. Wang, W. Li and Y.-Y. Yang, *Analyst*, 2016, **141**, 4502.

6 (*a*) H.-R. Wang, J.-H. Qin, C. Huang, Y.-B. Han, W.-J. Xu and H.-W. Hou, *Dalton Trans.*, 2016, **45**, 12710; (*b*) X.-J. Liu, Y.-H. Zhang, Z. Chang, A.-L. Li, D. Tian, Z.-Q. Yao, Y.-Y. Jia and X.-H. Bu, *Inorg. Chem.*, 2016, **55**, 7326; (*c*) B.-L. Li, H.-N. Wang, L. Zhao, G.-Z. Li and Z.-M. Su, *Inorg. Chem. Commun.*, 2016, **66**, 87; (*d*) L.-N. Zhang, C. Zhang, B. Zhang, C.-X. Du and H.-W. Hou, *CrystEngComm*, 2015, **17**, 2837; (*e*) H.-N. Wang, S.-Q. Jiang, Q.-Y. Lu, Z.-Y. Zhou, S.-P. Zhuo, G.-G. Shan and Z.-M. Su, *RSC Adv.*, 2015, **5**, 48881; (*f*) Y.-X. Shi, F.-L. Hu, W.-H. Zhang and J.-P. Lang, *CrystEngComm*, 2015, **17**, 9404; (*g*) F.-Y. Yi, W.-T. Yang and Z.-M. Sun, *J. Mater. Chem.*, 2012, **22**, 23201.

7 Y. Li, H. Song, Q. Chen, K. Liu, F.-Y. Zhao, W.-J. Ruan and Z. Chang, *J. Mater. Chem. A*, 2014, **2**, 9469.

8 Bruker AXS, *SAINT Software Reference Manual*, Madison, WI, 1998.

9 G. M. Sheldrick, *SHELXL97, Program for Crystal Structure Refinement*, University of Göttingen, Göttingen, Germany, 1997.

10 A. L. Spek, *J. Appl. Crystallogr.*, 2003, **36**, 7.

11 H. F. Brito, O. L. Malta, M. C. F. C. Felinto, E. E. S. Teotonio, J. F. S. Menezes, C. F. B. Silva, C. S. Tomiyama and C. A. A. Carvalho, *J. Alloys Compd.*, 2002, **344**, 293.

12 (*a*) Q. Liu, J.-M. Yang, F. Guo, L.-N. Jin and W.-Y. Sun, *Dalton Trans.*, 2016, **45**, 5841; (*b*) Z.-M. Hao, G.-C. Yang, X.-Z. Song, M. Zhu, X. Meng, S.-N. Zhao, S.-Y. Song and H.-J. Zhang, *J. Mater. Chem. A*, 2014, **2**, 237.

13 Z.-Q. Shi, Z.-J. Guo and H.-G. Zheng, *Chem. Commun.*, 2015, **51**, 8300.